Robust Synthesis of Nanostructures

Tirthankar Dasgupta[†], Christopher Ma[‡], V. Roshan Joseph[†],
Z. L. Wang[‡], C. F. Jeff Wu[†]*

[†]*School of Industrial and Systems Engineering*,

[‡]*School of Materials Science and Engineering* ,

Georgia Institute of Technology, Atlanta, GA

**Corresponding author*

Abstract

An effort is made to systematically investigate the best process conditions that ensures synthesis of different types of one dimensional cadmium selenide nanostructures with high yield and reproducibility. Through a designed experiment and rigorous statistical analysis of experimental data, models linking the probabilities of obtaining specific morphologies to the process variables are developed. A new iterative algorithm for fitting a multinomial GLM is proposed and used. The optimum process conditions, which maximize the above probabilities and make the synthesis process robust (i.e., less sensitive) to variations of process variables around set values, are derived from the fitted models using Monte-Carlo simulations.

Cadmium Selenide (CdSe) has been found to exhibit one-dimensional morphologies of nanowires, nanobelts and nanosaws, often with the three morphologies being intimately intermingled within the as-deposited material. A slight change in growth condition can result in a totally different morphology. In order to identify the optimal

process conditions that maximize the yield of each type of nanostructure and, at the same time, make the synthesis process robust (i.e., less sensitive) to variations of process variables around set values, a large number of trials were conducted with varying process conditions. Here, the response is a vector whose elements correspond to the numbers of appearance of different types of nanostructures. The fitted statistical models would enable nano-manufacturers to identify the probability of transition from one nanostructure to another when changes, even of the slightest order, are made in one or more process variables. Inferential methods associated with the modeling procedure help in judging the relative impact of the process variables and their interactions on the growth of different nanostructures. Owing to the presence of internal noise, i.e., variation around the set value, each predictor variable is a random variable. Using Monte-Carlo simulations, the mean and variance of transformed probabilities are expressed as functions of the set points of the predictor variables. The mean is then maximized to find the optimum set values of the process variables, with the constraint that the variance is under control.

KEY WORDS: Nanotechnology, Statistical modeling, Robust Design, Cadmium Selenide nanostructures, Multinomial, Generalized Liner Model.

1 Introduction

Nanotechnology is the construction and use of functional structures designed from atomic or molecular scale with at least one characteristic dimension measured in nanometers (one nanometer = 10^{-9} meter, which is about 1/50,000 of the width of human hair). The size of these nanostructures allows them to exhibit novel and significantly improved physical, chemical, and biological properties, phenomena, and processes. Nanotechnology can provide unprecedented understanding about materials and devices and is likely to impact many fields. By using structure at nanoscale as a tunable physical variable, scientists can greatly expand the range of performance of existing chemicals and materials. Alignment of linear molecules in an ordered array on a substrate surface (self-assembled monolayers) can function as a new generation of chemical and biological sensors. Switching devices and functional units

at nanoscale can improve computer storage and operation capacity by a factor of a million. Entirely new biological sensors facilitate early diagnostics and disease prevention of cancers. Nanostructured ceramics and metals have greatly improved mechanical properties, both in ductility and strength.

Current research by nanoscientists typically focuses on novelty, discovering new growth phenomena and new morphologies. However, within the next five years there will likely be a shift in the nanotechnology community towards controlled and large-scale synthesis with high yield and reproducibility. This transition from laboratory-level synthesis to large scale, controlled and designed synthesis of nanostructures necessarily demands systematic investigation of the manufacturing conditions under which the desired nanostructures are synthesized *reproducibly*, in *large* quantity and with *controlled* or isolated morphology. This investigation must be systematic and complete, which is possible only by using statistical modeling and analysis of data obtained from carefully designed experiments. The implementation of statistical techniques offers the unique advantage of observing and quantifying *subtle* changes in the growth of a particular nanostructure as a function of the process variables. Such slight changes in the growth can easily be overlooked in the current methodology of nanomaterial characterization, possibly leading to inaccurate conclusions and missed opportunities regarding the control of growth mechanism. This is one of the reasons that make this statistical approach to nanomaterial synthesis potentially important; the other important reason being the need of making the synthesis process *robust*, i.e., insensitive to uncontrollable or noise factors.

Research in synthesizing semiconducting nanostructures is a forefront area in nanotechnology due to their applications in nanoelectronics, photonics, data storage, and sensing (Tolbert and Alivisatos 1994; Ma, Moore, Ding, Li and Wang 2004; Tran, Goldman, Anderson, Mauro and Mattoussi 2002). In particular, one-dimensional (1D) nanostructures present the ability to experimentally address the fundamental issues of reduced dimensionality and quantum confinement in one dimension (Lieber 1998; Alivisatos, Levinos, Steigerwald and Brus 1988). Cadmium selenide (CdSe) has been investigated over the past decade for applications in optoelectronics (Hodes, Albu-Yaron, Decker and Motisuke 1987), luminescent

materials (Bawendi, Kortan, Steigerwald and Brus 1989), lasing materials (Ma, Ding, Moore, Wang and Wang 2004) and biomedical imaging. It is the most extensively studied quantum-dot material and is therefore regarded as the model system for investigating a wide range of nanoscale processes. CdSe is found to exhibit 1D morphologies of nanowires, nanobelts and nanosaws (Ma and Wang 2005), often with the three morphologies being intimately intermingled together within the as-deposited material. This article reports a systematic study on the growth of 1D CdSe nanostructures through statistical analysis techniques, which are applied for modeling and optimizing the experimental parameters required for synthesizing desired nanostructures. This work has been done based on the experimental data presented in this paper and research published in Ma and Wang (2005).

Three types of nanostructures, viz. nanosaws, nanowires and nanobelts, are observed in the synthesis process. Images of these three nanostructures obtained using scanning electron microscope are shown in Figure 1. In this experiment, the response is a vector whose elements correspond to the numbers of appearance of different types of nanostructures and hence is a multinomial random variable. Thus a multinomial generalized linear model (GLM) is the appropriate tool for analyzing the experimental data and expressing the multinomial logits as functions of the predictor variables (McCullagh and Nelder 1989; Faraway 2006). A new iterative algorithm for fitting multinomial GLM that has certain advantages over the existing methods is proposed and implemented. The probability of obtaining each nanostructure is expressed as a function of the predictor variables. Owing to the presence of inner noise, i.e., variation around the set value, each predictor variable is a random variable. Using Monte-Carlo simulations, the expectation and variance of transformed probabilities are expressed as functions of the set points of the predictor variables. The expectation is then maximized to find the optimum set values of the process variables, ensuring at the same time that the variance is under control. The idea is thus similar to the two-step robust parameter design for larger-the-better responses (Wu and Hamada 2000, chap. 10).

The article is organized as follows. In Section 2, we give a brief account of the synthesis process. The experimental design and collection of data are described in Section 3. Section 4 is devoted to fitting of appropriate statistical models to the experimental data. This section

consists of two subsections. In Section 4.1 a preliminary analysis using a binomial GLM is shown. Estimates of the parameters obtained here are used as initial estimates in the iterative algorithm for multinomial GLM, which is developed and described in Section 4.2. In Section 5, we study the optimization of the process variables to maximize the expected yield of each nanostructure. The impact of this research and some concluding remarks are discussed in Section 6.

2 The synthesis process

The CdSe nanostructures were synthesized through a thermal evaporation process in a single zone horizontal tube furnace (Thermolyne 79300). A 30-inch polycrystalline Al_2O_3 tube (99.9% purity) with an inner diameter of 1.5 inches was placed inside the furnace. Commercial grade CdSe (Alfa Aesar, 99.995% purity, metal basis) was placed at the center of the tube as use for a source material. Single-crystal silicon substrates with a 2-nanometer thermally evaporated non-continuous layer of gold were placed downstream of the source in order to collect the deposition of the CdSe nanostructures. Water-cooled aluminum endcaps were used to seal the system as a mechanical roughing pump purged the system of oxygen. After the chamber had maintained a pressure of 2×10^{-2} torr for an hour, the system temperature was raised to a designated set point at a rate of 20^0 C/min and a nitrogen carrier gas was sent through the system at a rate of 50 sccm. Although the primary function of the carrier gas was to transport the sublimated vapor to cooler regions of the furnace, the secondary function of the gas was to build up the initial pressure of the system as well as controlling the partial pressure of the vaporized source material. This ensured that the pressure of the system was constant throughout the entire synthesis process. The system was held at the set temperature and pressure for a period of 60 minutes and cooled to room temperature afterwards. The as-deposited products were characterized and analyzed by scanning electron microscopy (SEM) (LEO 1530 FEG), transmission electron microscopy (TEM) (Hitachi HF-2000 FEG at 200 kV). 180 individual nanostructures were counted from the deposition on each substrate.

A schematic diagram of the synthesis process is shown in Figure 2.

3 Design of experiment and data collection

The two key process variables affecting morphology of CdSe nanostructures are temperature and pressure. A 5×9 full factorial experiment was conducted with five levels of source temperature (630, 700, 750, 800, 850^0 C) and nine levels of pressure (4, 100, 200, 300, 400, 500, 600, 700, 800 mbar). For a specific combination of source temperature and pressure, 4-6 substrates were placed downstream of the source to collect the deposition of nanostructures. The distance of the mid-point of the substrate from the source was measured and treated as a covariate.

Three experimental runs were conducted with each of the 45 combinations of temperature and pressure. However, these three runs cannot be considered to be replicates, since the number and location of substrates were not the same in the three runs. Consider, for example, the three runs performed with a temperature of 630^0 C and pressure of 4 mb. In the first run, six substrates were placed at distances of 1.9, 4.2, 4.9, 6.4, 8.1, 10.2 cm from the source. In the second run, four substrates were placed at distances of 1.7, 4.6, 7.1, 8.9 cm from the source. Seven substrates were placed at distances of 2.0, 4.3, 4.9, 6.4, 8.5, 10.6, 13.0 cm from the source in the third run. Therefore 17 (=6+4+7) individual substrates were obtained with the temperature and pressure combination of (630^0 C, 4 mb). Each of these 17 substrates constitute a row in Table 1. The total number of substrates obtained from the 135 ($=45 \times 3$) runs was 415. Note that this is not a multiple of 45 owing to an unequal number of substrates corresponding to each run.

Considering each of the 415 substrates as an experimental unit, the design matrix can thus be considered to be a 415×3 matrix, where the three columns correspond to source temperature ($TEMP$), pressure($PRES$) and distance from the source ($DIST$). Each row corresponds to a substrate, on which a deposition is formed with a specific combination of $TEMP, PRES$ and $DIST$ (see Table 1).

Recall that from the deposition on each substrate, 180 individual nanostructures were

counted using SEM images. The response was thus a vector $\mathbf{Y} = (Y_1, Y_2, Y_3, Y_4)$, where Y_1, Y_2, Y_3, and Y_4 denote respectively the number of nanosaws, nanowires, nanobelts and no morphology, with $\sum_{j=1}^{4} Y_j = 180$. For demonstration purposes, the first 29 rows of the complete data are shown in Table 1. These rows correspond to the temperature-pressure combinations (630,4) and (630,100). The complete data can be downloaded from www.isye.gatech.edu/∼roshan.

It was observed that, at a source temperature of 850^0 C, almost no morphology was observed. Therefore, results obtained from the 67 experimental units involving this level of temperature were excluded and the data for the remaining 348 units were considered for analysis.

Henceforth, we shall use the suffixes 1,2,3 and 4 to represent quantities associated with nanosaws, nanowires, nanobelts and no growth respectivly.

4 Model fitting

4.1 Individual modeling of the probability of obtaining each nanostructure using binomial GLM

Here, the response is considered binary, depending on whether we get a specific nanostructure or not. Let p_1, p_2 and p_3 denote respectively the probabilities of getting a nanosaw/nanocomb, nanowire and nanobelt. Then, for $j = 1, 2, 3$, the marginal distribution of Y_j is binomial with $n = 180$ and probability of success p_j. The log-odds ratio of obtaining the j^{th} type of morphology is given by

$$\zeta_j = \log \frac{p_j}{1 - p_j}.$$

Our objective is to fit a model that expresses the above log-odds ratios in terms $TEMP$, $PRES$ and $DIST$.

From the main effects plot of $TEMP$, $PRES$ and $DIST$ against observed proportions of nanosaws, nanowires and nanobelts (Figures 3a, 3b and 3c), we observe that a quadratic

model should be able to express the effect of each variable on p_j adequately. The interaction plots (interaction plots for nanosaws shown in Figures 4a-4c) give a preliminary impression that all the three two-factor interactions are likely to be important. We therefore decide to fit a quadratic response model to the data.

For each process variable X, we use the transformation $Y = 2\big(X - \min(X)\big)/\big(\max(X) - \min(X)\big) - 1$, so that the range of each transformed process variable is $[-1, 1]$. Let T, P and D denote the scaled variables obtained by transforming $TEMP$, $PRES$ and $DIST$ respectively.

Using a binomial GLM with a logit link (McCullagh and Nelder, 1989), we obtain the following models that express the log-odds ratios of getting a nanosaw/nanocomb, nanowire and nanobelt as functions of T, P, D :

$$\begin{aligned}\hat{\zeta}_1 = \; & - \; 0.99 - 0.29 \;\; T - 1.52 \;\; P - 2.11 \;\; D - 0.95 \;\; T^2 - 1.30 \;\; P^2 - 5.64 \;\; D^2 \\ & - \; 0.18 \;\; TP - 1.03 \;\; PD + 4.29 \;\; TD, \end{aligned} \tag{1}$$

$$\begin{aligned}\hat{\zeta}_2 = \; & - \; 0.56 + 0.82 \;\; T - 2.53 \;\; P - 1.59 \;\; D - 0.58 \;\; T^2 - 2.04 \;\; P^2 - 2.62 \;\; D^2 \\ & + \; 1.17 \;\; TP - 1.44 \;\; PD + 0.87 \;\; DT, \end{aligned} \tag{2}$$

$$\begin{aligned}\hat{\zeta}_3 = \; & - \; 1.68 + 0.19 \;\; T - 1.88 \;\; P - 0.58 \;\; D - 1.69 \;\; T^2 - 0.34 \;\; P^2 - 3.20 \;\; D^2 \\ & + \; 0.87 \;\; TP - 0.94 \;\; PD - 2.58 \;\; TD. \end{aligned} \tag{3}$$

All the terms are seen to be highly significant. The residual plots for all the three models do not exhibit any unusual pattern.

4.2 Simultaneous modeling of the probability vector using multinomial GLM

Denoting the probability of not obtaining any nanostructure by p_4, we must have $\sum_{j=1}^{4} p_j = 1$. Although the results obtained by using the binomial GLM are easily interpretable and useful, the method suffers from the inherent drawback that, for specific values of T, P and D, the fitted values of the probabilities may be such that $\sum_{j=1}^{3} p_j > 1$. This is due to the fact that the *correlation* structure of $\mathbf{Y}$ is completely ignored in this approach.

A more appropriate modeling strategy is to utilize the fact that the response vector $\mathbf{Y}$ follows a multinomial distribution with $n = 180$ and probability vector $\mathbf{p} = (p_1, p_2, p_3, p_4)$. In this case, one can express the multinomial logits $\eta_j = \log(\frac{p_j}{p_4}), j = 1, 2, 3$ as functions of T, P and D. Note that η_j can be easily interpreted as the logg-odds ratio of obtaining the j^{th} morphology as compared to no nanostructure, with $\eta_4 = 0$.

One method for fitting such nominal response models (Aitkin, Anderson, Francis and Hinde 1989) is to create a pseudo factor with a level for each data point, and use a Poisson GLM with log link. This method, although appropriate for small data sets, becomes cumbersome when the number of data points is large. In the presence of a large number of levels of the pseudo factor, a large part of the output generated by standard statistical softwares like R becomes redundant, because only the terms involving interaction between the categories and the predictor variables are of interest. Faraway (2006) points out some practical inconveniences of using this method. Its application to the current problem clearly becomes very cumbersome owing to the large number (348) of data points.

An alternative method is to obtain the parameter estimates by direct maximization of the multinomial likelihood function. One such algorithm provided by Venebles and Ripley (2002), and implemented in statistical softwares R and S-PLUS, optimizes the likelihood function using a neural network model.

We propose a new iterative method of fitting multinomial logit models. The method is very intuitive and is based on an iterative application of binomial GLM. Owing to some simple properties, testing significance of terms included in the model and, consequently, variable selection becomes a very simple task. We develop the method in the next few

paragraphs.

Let $\mathbf{Y}_i = (Y_{i1}, \ldots, Y_{i4})$ denote the response vector corresponding to the i^{th} data point, $i = 1$ to N. Let $n_i = \sum_{j=1}^{4} Y_{ij}$. Here, $N = 348$ and $n_i = n = 180$ for all i. We have,

$$P(Y_{i1} = y_{i1}, \ldots, Y_{i4} = y_{i4}) = \frac{n_i!}{y_{i1}! \ldots y_{i4}!} p_{i1}^{y_{i1}} \ldots p_{i4}^{y_{i4}}.$$

Thus the likelihood function is given by

$$\begin{aligned} L(\mathbf{Y}_1, \ldots, \mathbf{Y}_N) &= \prod_{i=1}^{N} \frac{n_i!}{y_{i1}! \ldots y_{i4}!} p_{i1}^{y_{i1}} \ldots p_{i4}^{y_{i4}} \\ &= \prod_{i=1}^{N} \frac{n_i!}{y_{i1}! \ldots y_{i4}!} \prod_{j=1}^{3} \left(\frac{p_{ij}}{p_{i4}}\right)^{y_{ij}} p_{i4}^{\sum_{j=1}^{4} y_{ij}}. \end{aligned}$$

Defining $\eta_{ij} = \log \frac{p_{ij}}{p_{i4}}$, we have

$$p_{ij} = \frac{\eta_{ij}}{1 + \sum_{j=1}^{3} \exp(\eta_{ij})} \quad j = 1, 2, 3, \tag{4}$$

and

$$p_{i4} = \frac{1}{1 + \sum_{j=1}^{3} \exp(\eta_{ij})}. \tag{5}$$

Therefore the log-likelihood can be written as

$$\begin{aligned} \log(L) &= \sum_{i=1}^{N} \left(\log n_i! - \sum_{j=1}^{4} \log y_{ij}! + \sum_{j=1}^{3} y_{ij} \log \frac{p_{ij}}{p_{i4}} + n_i \log p_{i4} \right) \\ &= \sum_{i=1}^{N} \left(\log n_i! - \sum_{j=1}^{4} \log y_{ij}! + \sum_{j=1}^{3} y_{ij} \eta_{ij} - n_i \log \left(1 + \sum_{j=1}^{3} \exp(\eta_{ij})\right) \right). \end{aligned} \tag{6}$$

Let $\mathbf{x}_i = (1, T_i, P_i, D_i, T_i^2, P_i^2, D_i^2, T_iP_i, P_iD_i, T_iD_i)', i = 1, \ldots, N$. The objective is to express the η's as functions of $\mathbf{x}$. Substituting $\eta_{ij} = \mathbf{x}_i' \boldsymbol{\beta}_j$ in (6) and successively differentiating with respect to each $\boldsymbol{\beta}_j$, we get the maximum likelihood (ML) equations as

$$\sum_{i=1}^{N} \mathbf{x}_i \left(y_{ij} - n_i \frac{\exp(\eta_{ij})}{1 + \sum_{j=1}^{3} \exp(\eta_{ij})} \right) = \mathbf{0}, \quad j = 1, 2, 3, \tag{7}$$

$$\sum_{i=1}^{N} \mathbf{x}_i \left(y_{14} - n_i \frac{1}{1 + \sum_{j=1}^{3} \exp(\eta_{ij})} \right) = \mathbf{0}, \tag{8}$$

where $\mathbf{0}$ denotes a vector of zeros having length 10. Writing $\exp(\gamma_{il}) = \left(1+\sum_{l\neq j}\exp(\eta_{ij})\right)^{-1}$, we obtain from (7)

$$\sum_{i=1}^{N}\mathbf{x}_i\left(y_{ij} - n_i\frac{\exp(\eta_{ij}+\gamma_{ij})}{1+\exp(\eta_{ij}+\gamma_{ij})}\right) = \mathbf{0},\ \ j=1,2,3. \tag{9}$$

Note that each equation in (9) is the ML equation of a binomial GLM with logit link. Thus, if some initial estimates of $\boldsymbol{\beta}_2, \boldsymbol{\beta}_3$ are available, and consequently γ_{i1} can be computed, then $\boldsymbol{\beta}_1$ can be estimated by fitting a binomial GLM of Y_1 on $\mathbf{x}$. Similarly, $\boldsymbol{\beta}_2$ and $\boldsymbol{\beta}_3$ can be estimated. The following algorithm is thus proposed.

Binomial GLM-based iterative algorithm for fitting a multinomial GLM :

Let $\boldsymbol{\beta}_j^{(k)}$ be the estimate of $\boldsymbol{\beta}_j, j=1,2,3$, at the end of the k^{th} iteration.

Step 1. Using $\boldsymbol{\beta}_2^{(k)}$ and $\boldsymbol{\beta}_3^{(k)}$, compute $\eta_{i2}^{(k)} = \mathbf{x}_i'\boldsymbol{\beta}_2^{(k)}$ and $\eta_{i3}^{(k)} = \mathbf{x}_i'\boldsymbol{\beta}_3^{(k)}$ for $i=1,\ldots,n$.

Step 2. Compute $\gamma_{i1}^{(k)} = \log\frac{1}{1+\exp(\eta_{i2}^{(k)})+\exp(\eta_{i3}^{(k)})}, \quad i=1,\ldots,n.$

Step 3. Treating Y_1 as the response and using the same design matrix, fit a binomial GLM with logit link. The vector of coefficients thus obtained is $\boldsymbol{\beta}_1^{(k+1)}$.

Step 4. Repeat steps 1-3 by successively updating γ_{i2} and γ_{i3} and estimating $\boldsymbol{\beta}_2^{(k+1)}$ and $\boldsymbol{\beta}_3^{(k+1)}$

Repeat steps 1-4 until convergence. A proof of convergence is given in Appendix 1. Note that we use the 'offset' command in statistical software R to separate the coefficients associated with η_1 from those with γ_1.

To obtain the initial estimates $\widehat{\eta}_{i2}^{(0)}$ and $\widehat{\eta}_{i3}^{(0)}$, we use the results obtained from the binomial GLM as described in Section 4.1. Let

$$\log\frac{\widehat{p}_{ij}}{1-\widehat{p}_{ij}} = \mathbf{x}_i'\widehat{\boldsymbol{\delta}}_j, \tag{10}$$

where $\widehat{\boldsymbol{\delta}}_j$ is obtained by using binomial GLM. Recalling the definition of η_{ij}, the initial estimates are obtained as

$$\widehat{\eta}_{ij}^{(0)} = \log\frac{\widehat{p}_{ij}}{1-\sum_{l=1}^{3}\widehat{p}_{il}},\ \ j=2,3, \tag{11}$$

where $\widehat{p}_{il}, l = 1, 2, 3$ are estimated from (10). It is possible, however, that for some i, $\sum_{l=1}^{3} \widehat{p}_{il} = \pi_i \geq 1$. For those data points, we provide a small correction as follows:

$$\widehat{p}_{il}(corrected) = \begin{cases} \frac{\widehat{p}_{il}}{\pi_i}(1 - \frac{1}{2n_i}) & , l = 1, 2, 3 \\ \frac{1}{2n_i} & , l = 4 \end{cases} .$$

To justify the correction, we note that it is a common practice to give a correction of $\frac{1}{2n_i}$ (Cox 1970, chap. 3) in estimation of probabilities from binary data. The correction given to category 4 is adjusted among the other three categories in the same proportion as the estimated probabilities. This ensures that $\widehat{p}_{il} > 0$ for all i and $\sum_{l=1}^{4} \widehat{p}_{il} = 1$

In this example, there were 18 data points (out of 348) corresponding to which we had $\sum_{l=1}^{3} \widehat{p}_{il} \geq 1$. Following the procedure described above to obtain the initial estimates, convergence was achieved after the 27^{th} iteration. The fitted models are given below:

$$\begin{aligned} \widehat{\eta_1} = \quad & 0.42 - 0.12\ T - 3.08\ P - 3.68\ D - 1.84\ T^2 - 1.52\ P^2 - 9.09\ D^2 \\ + \quad & 0.60\ TP - 2.31\ PD + 5.75\ TD, \end{aligned} \tag{12}$$

$$\begin{aligned} \widehat{\eta_2} = \quad & 0.54 + 0.88\ T - 3.85\ P - 3.13\ D - 1.21\ T^2 - 2.28\ P^2 - 5.26\ D^2 \\ + \quad & 1.83\ TP - 2.62\ PD + 2.07\ TD, \end{aligned} \tag{13}$$

$$\begin{aligned} \widehat{\eta_3} = \ - \quad & 0.10 + 0.39\ T - 3.67\ P - 2.51\ D - 2.51\ T^2 - 1.12\ P^2 - 7.07\ D^2 \\ + \quad & 1.72\ TP - 2.38\ PD + 4.47\ TD. \end{aligned} \tag{14}$$

Inference for the proposed method:

To test the significance of the terms in the model, one can use the asymptotic normality of the maximum likelihood estimates. Let $\mathbf{H}_\beta$ denote the 30×30 matrix consisting of the negative expectations of second-order partial derivatives of the log-likelihood function in (6), the derivatives being taken with respect to the components of $\boldsymbol{\beta}_1, \boldsymbol{\beta}_2$ and $\boldsymbol{\beta}_3$. Denoting the final estimator of $\boldsymbol{\beta}$ as $\boldsymbol{\beta}^*$, the estimated asymptotic variance-covariance matrix of the estimated model coefficients is given by $\boldsymbol{\Sigma}_{\beta^*} = \mathbf{H}_{\beta^*}{}^{-\mathbf{1}}$. For a specific coefficient β_l, the null hypothesis $H_0 : \beta_l = 0$ can be tested using the test statistic $z = \widehat{\beta}_l / s(\widehat{\beta}_l)$, where $s^2(\widehat{\beta}_l)$ is the l^{th} diagonal element of $\boldsymbol{\Sigma}_{\beta^*}$.

Let $\beta_l^{(k)}$ denote the estimate of β_l obtained after the k^{th} iteration of the proposed algorithm. Let $s^2(\beta_l^{(k)})$ denote the estimated asymptotic variance of $\beta_l^{(k)}$. It can easily be seen (Appendix 2) that $s^2(\beta_l^{(k)})$ converges to $s^2(\beta_l^*)$. Thus, as the parameter estimates converge to the maximum likelihood estimates, their standard errors also converge to the standard error of the MLE. More generally, if $\mathbf{\Sigma}_{\beta(\mathbf{k})}$ denotes the asymptotic covariance matrix of the parameter estimates at the end of the k^{th} iteration, then $\mathbf{\Sigma}_{\beta(\mathbf{k})} \longrightarrow \mathbf{\Sigma}_{\beta^*}$.

The above property of the proposed algorithm ensures that one does not have to spend any extra computational effort in judging the significance of the model terms. The binomial GLM function in R used in every iteration automatically tests the significance of the model terms, and the p-values associated with the estimated coefficients after convergence can be used for inference. Thus, the inferential procedures and diagnostic tools of the binomial GLM can easily be used in the multinomial GLM model. This is clearly an advantage of the proposed algorithm over existing methods. Further, the three models for nanosaws, nanobelts and nanowires can be compared using these diagnostic tools. Such facilities are not available in the current implementation of the R and S-plus based algorithms (Faraway 2006).

The z values corresponding to the 30 coefficients are presented in Table 2. The p values are not included in the table as each of them is of the order 10^{-6} or less. All the 30 terms are seen to be highly significant. To check the model adequacy, we use the generalized R^2 statistic derived by Naglekerke (1991) defined as $R^2 = \big(1-\exp\left((D - D_{null})/n\right)\big)/\big(1-\exp\left(-D_{null}/n\right)\big)$, where D and D_{null} denote the residual deviance and the null deviance respectively. The R^2 associated with the models for nanosaws, nanowires and nanobelts are obtained as 61%, 50% and 76% respectively. This shows that that the prediction error associated with the model for nanowires is the largest. This finding is consistent with the observation made by Ma and Wang (2005) that growth of nanowires is less restrictive compared to nanosaws and nanowires, and can be carried out at wide ranges of temperature and pressure.

5 Optimization of the synthesis process

In the previous subsections, the three process variables have been treated as non-stochastic. However, in reality, none of these variables can be controlled precisely and each of them exhibits certain fluctuations around the set (nominal) value. Such fluctuation is a form of noise, called internal noise (Wu and Hamada 2000, chap. 10) associated with the synthesis process and needs to be considered in performing optimization.

It is therefore reasonable to consider $TEMP$, $PRES$ and $DIST$ as random variables. Let μ_{TEMP}, μ_{PRES}, μ_{DIST} denote the set values of $TEMP$, $PRES$ and $DIST$ respectively. Then we assume

$$TEMP \sim N(\mu_{TEMP}, \sigma^2_{TEMP}),$$
$$PRES \sim N(\mu_{PRES}, \sigma^2_{PRES}),$$
$$DIST \sim N(\mu_{DIST}, \sigma^2_{DIST}).$$

where σ^2_{TEMP}, σ^2_{PRES}, σ^2_{DIST} are the respective variances of $TEMP$, $PRES$ and $DIST$ around their set values and are estimated from process data (Section 5.1). The task now is to determine the optimal nominal values μ_{TEMP}, μ_{PRES} and μ_{DIST} so that the expected yield of each nanostructure is maximized subject to the condition that the variance in yield is acceptable.

5.1 Measurement of internal noise in the synthesis process

Some surrogate process data collected from the furnace were used for estimation of the above variance components. Temperature and pressure were set at specific levels (those used in the experiment), and their actual values were measured repeatedly over a certain period of time. The range of temperature and pressure corresponding to each set value was noted. The variation in distance, which is due to repeatability and reproducibility errors associated with the measurement system, was assessed separately. The summarized data in Table 3 show the observed ranges of $TEMP$, $PRES$ and $DIST$ against different nominal values. Under the assumption of normality, the range can be assumed to be approximately equal to six times the standard deviation.

We observe from Table 3 that, for the process variable $DIST$, the range of values around the nominal μ_{DIST} is a constant ($2 \times 0.02 = 0.04$ mm) and independent of μ_{DIST}. Equating this range to $6\sigma_{DIST}$, we obtain an estimate of σ_{DIST} as $0.04/6 = 0.067$ mm.

Similarly, for $TEMP$, the range can be taken to be almost a constant. Equating the mean range of 12.8 ($=2 \times (2 \times 7 + 3 \times 6)/5$) degrees to $6\sigma_{TEMP}$, an estimate of σ_{TEMP} is obtained as $12.8/6 = 2.13$ degree C.

The case of $PRES$ is, however, different. The range, and hence σ_{PRES} is seen to be an increasing function of μ_{PRES}. Corresponding to each value of μ_{PRES}, an estimate of σ_{PRES} is obtained by dividing the range by 6. Using these values of σ_{PRES}, the following regression line is fitted through the origin to express the relationship between σ_{PRES} and μ_{PRES}

$$\sigma_{PRES} = 0.025\mu_{PRES}. \tag{15}$$

Recall that all the models are fitted with the transformed variables T, P, D. Each transformed variable Y was obtained from the original variable X by a transformation of the form $a + bX$, where $a = 2X/\big(\max(X) - \min(X)\big)$ and $b = -\big(\max(X) + \min(X)\big)/\big(\max(X) - \min(X)\big)$. Hence, $\mu_Y = a + b\mu_X$ and $\sigma_Y = |b|\sigma_X$. Thus, we have,

$$\begin{aligned}
T &\sim N(\mu_T, \sigma_T^2), \text{ where } \mu_T = -8.4 + 0.012\mu_{TEMP} \text{ and } \sigma_T = 0.012\sigma_{TEMP}\ , \\
P &\sim N(\mu_P, \sigma_P^2), \text{ where } \mu_P = -1.01 + 0.0025\mu_{PRES}, \text{ and } \sigma_P = 0.0025\sigma_{PRES}, \\
D &\sim N(\mu_D, \sigma_D^2), \text{ where } \mu_D = -23.6 + 0.0154\mu_{DIST} \text{ and } \sigma_D = 0.0154\sigma_{DIST}.
\end{aligned}$$

5.2 Obtaining the mean and variance functions of p_1, p_2, p_3

From (4), we have the estimated probability functions as $\widehat{p_j} = \exp(\widehat{\eta_j})/\big(1 + \sum_{j=1}^{3} \exp(\widehat{\eta_j})\big)$, where $\widehat{\eta_j}$ are given by (12)-(14).

Expressing $E(p_j)$ and $Var(p_j)$ in terms of μ_T, μ_P, μ_D is not a straightforward task. To do this, we use Monte Carlo simulations. For each of the 180 combinations of $\mu_{TEMP}, \mu_{PRES}, \mu_{DIST}$ ($\mu_{TEMP} = 630, 700, 750, 800$; $\mu_{PRES} = 4, 100, 200, \ldots, 800$; $\mu_{DIST} = 12, 14, 16, 18, 20$) the following are done:

1. μ_T, μ_P and μ_D are obtained by appropriate transformation.

2. 5000 observations on T, P and D are generated from the respective normal distributions and η_j is obtained using equation (12), (13) or (14).

3. From the η_j values thus obtained, p_j's are computed using (4) and transformed to $\zeta_j = log\frac{p_j}{1-p_j}$.

4. The mean and variance of those 5000 ζ_j values (denoted by $\overline{\zeta_j}$ and $s^2(\zeta_j)$ respectively) are computed.

5. Using linear regression, $\bar{\zeta_j}$ and $\log s^2(\zeta_j)$ are expressed in terms of μ_T, μ_P and μ_D.

5.3 Maximizing the average yield

Since the response here is of larger-the-better type, maximizing the mean is more important than minimizing the variance in the two-step optimization procedure (Wu and Hamada 2000, chap. 10) associated with robust parameter design.

The problem can thus be formulated as :

$$\text{maximize } \overline{\zeta_j} \qquad \text{subject to}$$

$$-1 \leq \mu_T \leq 1, \quad -1 \leq \mu_P \leq 1, \quad -1 \leq \mu_D \leq 1 \quad \text{for} \quad j = 1, 2, 3.$$

Physically, this would mean maximizing the average log-odds ratio of getting a specific morphology.

The following models are obtained from the simulated data:

$$\begin{aligned} \overline{\zeta_1} = & - 0.75 + 0.20\mu_T - 1.02\mu_P - 1.39\mu_D - 1.50\mu_T^2 - 3.54\mu_P^2 - 11.02\mu_D^2 \\ & + 1.58\mu_T\mu_P - 2.22\mu_P\mu_D + 8.41\mu_T\mu_D, \end{aligned} \tag{16}$$

$$\begin{aligned} \overline{\zeta_2} = & - 0.40 + 0.80\mu_T - 2.96\mu_P - 1.43\mu_D - 0.98\mu_T^2 - 2.45\mu_P^2 - 6.05\mu_D^2 \\ & + 1.87\mu_T\mu_P - 3.41\mu_P\mu_D + 2.13\mu_T\mu_D, \end{aligned} \tag{17}$$

$$\begin{aligned} \overline{\zeta_3} = & - 1.25 + 0.26\mu_T - 2.6\mu_P - 0.42\mu_D - 2.36\mu_T^2 - 1.24\mu_P^2 - 8.03\mu_D^2 \\ & + 1.74\mu_T\mu_P - 3.32\mu_P\mu_D + 4.57\mu_T\mu_D. \end{aligned} \tag{18}$$

Maximizing these three functions using the *optim* command in R, we get the optimal conditions for maximizing the expected yield of nanosaws, nanowires and nanobelts in terms of μ_T, μ_P and μ_D. These optimal values are transformed to the original units (i.e., in terms of μ_{TEMP}, μ_{PRES}, and μ_{DIST}) and are summarized in Table 4.

Contour plots of average and variance of the yield probabilities of nanosaws, nanowires and nanobelts against temperature and pressure (at optimal distances) are shown in Figures 5a to 5e. The pink regions on the left (average) panels and the blue regions on the right (variance) panels are robust regions that promote high yield with minimal variation. On the basis of these contour plots and the optimization output summarized in Table 4, the following conclusions can be drawn:

1. For nanosaws and nanowires, robustness of the synthesis process depends more on the choice of pressure than on the temperature. The process is seen to be fairly robust at a pressure below 400 mb, irrespective of source temperature.

2. For nanobelts, temperature affects robustness strongly, and for a pressure of less than 400 mb, the process is very robust only when the temperature is in close proximity of 700^0 C.

3. A temperature of around 630 degrees and pressure of 310 mb simultaneously maximizes the average and minimize the variance of probability of obtaiining nanosaws.

4. A temperature of around 700 degrees and pressure of around 120 degrees results in highest average yield for nanowires. Low variance is also observed in this region.

5. Highest yield of nanobelts is achieved at a temperature of 680 degrees and pressure of 4 mb for nanobelts. This is also a low-variance region.

6. There is a large temperature-pressure region (pink in Fig 5c) that promotes high and consistent yield of nanowires.

7. Highest yields of nanobelts and nanowires are achieved at higher distance (i.e., lower local temperature) as compared to nanosaws.

Except for the robustness-related conclusions, most of the above findings are summarized and discussed by Ma and Wang (2005). They also provide plausible and in-depth physical interpretations of some of the above phenomena.

6 Summary and concluding remarks

In this article, we report an early application of statistical techniques in nanotechnology research. In terms of reporting results of nanotechnology experiments, this methodology can be considered a significant advancement over the rudimentary data analysis methods using simple graphs, charts and summary statistics (e.g., Song, Wang, Riedo and Wang 2005; Ma and Wang 2005) that have been reported in the nanotechnology literature so far.

Apart from the advantages discussed earlier in this paper and mentioned by Ma and Wang (2005), this study demonstrates how statistical techniques can help in identifying important higher-order effects (like quadratic effects or complex interactions among process variables) and utilize such knowledge in fine-tuning the optimal synthesis conditions. This work is also an important step towards large-scale controlled synthesis of CdSe nanostructures, since in addition to determining conditions for high yield, it also identifies robust settings of the process variables that are likely to guarantee consistent output.

Here we discuss the specific features of the data arising from a specific nanotechnology experiment and use a multinomial model to express the probabilities of specific morphologies as functions of process variables. A new iterative algorithm which is more appropriate than conventional methods for the present problem, is proposed for fitting the multinomial model. Inner noise is incorporated into the fitted models and robust settings of process variables that maximize the expected yield of each type of nanostructure are determined.

Future research may consist of determining more efficient statistical designs for conducting experiments in nanotechnology research and using latent variable techniques to explore the mechanism of transition from one nanostructure to another.

Acknowledgements

The research of VRJ was supported by NSF grant DMI-0448774. The research of ZLW was supported by grants from NSF, DARPA and NASA.

Appendices

Appendix-1: Proof of Convergence of the proposed algorithm:

For simplicity, consider a single predictor variable and assume that $\eta_{ij} = \beta_j x_i$, where β_j is a scalar ($i = 1, 2, \ldots, N, j = 1, 2, 3$). Let $Q(\beta_1, \beta_2, \beta_3) = \sum_{i=1}^{N} \left(\sum_{j=1}^{3} y_{ij}\eta_{ij} - n_i \log\left(1 + \sum_{j=1}^{3} \exp\left(\eta_{ij}\right)\right)\right)$. Recall that $\beta_j^{(k)}$ denotes the estimate of β_j obtained after the k^{th} iteration. Then, it suffices to show that

(i) $Q(\beta_1, \beta_2, \beta_3)$ is a concave function of β_j, $j = 1, 2, 3$, and

(ii) $Q(\beta_1^{(k+1)}, \beta_2^{(k)}, \beta_3^{(k)}) \geq Q(\beta_1^{(k)}, \beta_2^{(k)}, \beta_3^{(k)})$.

It is easy to see that for $l = 1, 2, 3$,

$$\frac{\partial^2 Q}{\partial \beta_l^2} = -\sum_{i=1}^{N} \frac{n_i x_i^2 e^{\beta_l x_i}(1 + \sum_{j \neq l} e^{\beta_j x_i})}{(1 + \sum_{j=1}^{3} e^{\beta_j x_i})^2} \leq 0,$$

which proves the concavity of Q.

To prove (ii), we note that for given $\beta_2^{(k)}, \beta_3^{(k)}$ the solution for β_1 to the equation

$$\sum_{i=1}^{N} \left(y_{i1} - n_i \frac{e^{\beta_1 x_i}}{1 + e^{\beta_1 x_i} + \sum_{j=2}^{3} e^{\beta_j^{(k)} x_i}} \right) x_i = 0$$

maximizes $Q(\beta_1, \beta_2^{(k)}, \beta_3^{(k)})$.

From the first equation of (9) and steps 1-3 of the algorithm, we have

$$\sum_{i=1}^{N} \left(y_{i1} - n_i \frac{e^{\beta_1^{(k+1)} x_i}}{1 + e^{\beta_1^{(k+1)} x_i} + \sum_{j=2}^{3} e^{\beta_j^{(k)} x_i}} \right) x_i = 0,$$

which means $\beta_1^{(k+1)} = \arg\max Q(\beta_1, \beta_2^{(k)}, \beta_3^{(k)})$. Therefore (ii) holds.

Appendix-2: Proof of convergence of the estimated covariance matrix

Again, for simplicity, consider a single predictor variable and assume that $\eta_{ij} = \beta_j x_i$ where β_j is a scalar ($i = 1, 2, \ldots, N, j = 1, 2, 3$). Let $\beta_j^{(k)}$ denote the estimate of β_j obtained after steps 1-3 of the k^{th} iteration and β_j^* denote the final estimate of β_j obtained by the proposed algorithm.

The estimated asymptotic variance of $\beta_1^{(k)}$, denoted by $s^2(\beta_1^{(k)})$, is given by the negative expectation of $\frac{\partial^2 \log L_{b1}}{\partial \beta_1^2}|_{\beta_1^{(k)}, \beta_2^{(k-1)}, \beta_3^{(k-1)}}$, where $\log L_{b1}$ denotes the binomial log-likelihood function of $y_{i1} (i = 1, \ldots N)$ that corresponds to the first of the three equations in (9) and is given by

$$\log L_{b1} = \sum_{i=1}^{N} \log \binom{n}{y_{i1}} + \sum_{i=1}^{N} y_{i1}(\eta_{i1} + \gamma_{i1}) - n_i \sum_{i=1}^{N} \log \Big(1 + \exp(\eta_{i1} + \gamma_{i1})\Big).$$

Now, $s^2(\beta_1^*)$, the estimated asymptotic variance of β_1^*, is given by the negative expectation of $\frac{\partial^2 \log L}{\partial \beta_1^2}|_{\beta_j = \beta_j^*, j=1,2,3}$, where $\log L$ is the multinomial likelihood given by (6).

It can easily be seen that

$$\frac{\partial^2 \log L_{b1}}{\partial \beta_1^2} = -\sum_{i=1}^{N} n_i x_i^2 \frac{1 + \exp(\eta_{i2}) + \exp(\eta_{i3})}{\big(1 + \exp(\eta_{i1}) + \exp(\eta_{i2}) + \exp(\eta_{i3})\big)^2} = \frac{\partial^2 \log L}{\partial \beta_1^2}.$$

By convergence of $\beta_j^{(k)}$ to β_j^* for $j = 1, 2, 3$, it follows that $s^2(\beta_1^{(k)}) \longrightarrow s^2(\beta_1^*)$.

Similarly, each component in the covariance matrix $\mathbf{\Sigma}_{\beta^{(\mathbf{k})}}$ can be proven to converge to each component of $\mathbf{\Sigma}_{\beta^*}$.

References

Aitkin, M., Anderson, D.A., Francis, B.J. and Hinde, J.P. (1989), *Statistical Modelling in GLIM*, Clarendon Press, Oxford.

Alivisatos, A.P., Harris, A.L., Levinos, N.J., Steigerwald, M.L. and Brus, L.E. (1988), "Electronic States of Semiconductor Clusters: Homogeneous and Inhomogeneous Broadening of the Optical Spectrum," *Journal of Chemical Physics*, 89, 4001.

Bawendi, M.G., Kortan, A.R., Steigerwald, M.L., and Brus, L.E. (1989), "X-ray Structural Characterization of Larger Cadmium Selenide (CdSe) Semiconductor Clusters," *Journal of Chemical Physics*, 91, 7282-7290.

Cox, D.R. (1970), *Analysis of Binary Data*, London : Chapman & Hall.

Faraway, J.J. (2006), *Extending the Linear Model with R : Generalized Linear, Mixed Effects and Nonparametric Regression Models*, Boca Raton : Chapman & Hall/CRC.

Hodes, G., Albu-Yaren, A., Decker, F., Motisuke, P. (1987), "Three-Dimensional Quantum-Size Effect in Chemically Deposited Cadmium Selenide Films," *Physics Review B*, 36, 4215-4221.

Lieber, C.M. (1998), "One-Dimensional Nanostructures: Chemistry, Physics and Applications," *Solid State Communications*, 107, 607-616.

Ma, C., Moore, D.F., Ding, Y., Li, J. and Wang, Z.L. (2004), "Nanobelt and Nanosaw Structures of II-VI Semiconductors," *International Journal of Nanotechnology*, 1, 431-451.

Ma,C., Ding, Y., Moore, D.F., Wang, X. and Wang,Z.L. (2004), "Single-Crystal CdSe Nanosaws," *Journal of American Chemical Society*, 126, 708-709.

Ma, C. and Wang, Z.L. (2005), "Roadmap for Controlled Synthesis of CdSe Nanowires, Nanobelts and Nanosaws," *Advanced Materials*, 17, 1-6.

McCullagh, P. and Nelder, J. (1989). *Generalized Linear Models*, Chapman and Hall, London.

Naglekerke, N. (1991), "A Note on a General Definition of the Coefficient of Determination," *Biometrika*, 78, 691-692.

Song, J., Wang, X., Riedo, E. and Wang, Z.L. (2005), "Systematic Study on Experimental Conditions for Large-Scale Growth of Aligned ZnO Nanwires on Nitrides," *Journal of Physical Chemistry B*, 109, 9869-9872.

Tolbert, S.H. and A.P. Alivisatos, A.P. (1994), "Size Dependence of a First Order Solid-Solid Phase Transition: The Wurtzite to Rock Salt Transformation in CdSe Nanocrystals," *Science*, 265, 373-376.

Tran, P.T., Goldman, E.R., Anderson, G.P., Mauro, J.M. and Mattoussi, H. (2002),"Use of Luminescent CdSe-ZnS Nanocrystal Bioconjugates in Quantun Dot-Based Nanosensors,"*Physics Status Solidi B-Basic Research*, 229, 427-432.

Wu, C.F.J., and Hamada, M. (2000), *Experiments: Planning, Analysis, and Parameter Design Optimization*, New York: Wiley.

Venables, W.N. and Ripley, B.D. (2000), *Modern Applied Statistics with S-PLUS*, New York: Springer.

Table 1: Partial data (29 rows out of 415) obtained from the nano-experiment

Temperature	Pressure	Distance	Nanosaws	Nanowires	Nanobelts	No growth
630	4	12.4	0	0	0	180
630	4	14.7	74	106	0	0
630	4	15.4	59	121	0	0
630	4	16.9	92	38	50	0
630	4	18.6	0	99	81	0
630	4	20.7	0	180	0	0
630	4	12.2	50	94	36	0
630	4	15.1	90	90	0	0
630	4	17.6	41	81	58	0
630	4	19.4	0	121	59	0
630	4	12.5	49	86	45	0
630	4	14.8	108	72	0	0
630	4	15.4	180	0	0	0
630	4	16.9	140	40	0	0
630	4	19.0	77	47	56	0
630	4	21.1	0	88	92	0
630	4	23.5	0	0	0	180
630	100	12.1	0	0	0	180
630	100	15.8	92	74	0	14
630	100	18.4	0	180	0	0
630	100	20.1	0	0	0	180
630	100	12.3	0	92	88	0
630	100	15.0	14	144	22	0
630	100	17.1	31	113	36	0
630	100	19.5	0	0	0	180
630	100	12.1	85	59	36	0
630	100	15.4	65	74	41	0
630	100	18.0	0	180	0	0
630	100	19.9	0	0	0	180

Table 2: Computed values of the test statistic for each estimated coefficient

	Nanosaws ($\widehat{\eta_1}$)			Nanowires ($\widehat{\eta_2}$)			Nanobelts($\widehat{\eta_3}$)		
Term	$\hat{\beta}$	S.E.	z-val.	$\hat{\beta}$	S.E.	z-val.	$\hat{\beta}$	S.E.	z-val.
Intercept	0.42	0.03	15.82	0.54	0.02	23.97	-0.10	0.03	-3.22
T	-0.12	0.03	-3.65	0.88	0.03	34.89	0.39	0.05	7.89
P	-3.08	0.04	-68.66	-3.85	0.04	-86.37	-3.67	0.07	-56.20
D	-3.68	0.07	-49.53	-3.13	0.05	-62.62	-2.51	0.08	-29.67
T^2	-1.84	0.04	-49.29	-1.21	0.02	-50.36	-2.51	0.04	-57.94
P^2	-1.52	0.05	-31.02	-2.28	0.05	-49.55	-1.12	0.07	-16.18
D^2	-9.09	0.11	-82.71	-5.26	0.06	-90.73	-7.07	0.10	-71.75
TP	0.60	0.05	13.01	1.83	0.04	50.39	1.72	0.07	25.51
PD	-2.31	0.09	-25.21	-2.62	0.06	-42.03	-2.38	0.11	-22.28
TD	5.75	0.09	65.28	2.07	0.04	51.65	4.47	0.09	50.86

Table 3: Fluctuation of process parameters around set values

Temperature		Pressure		Distance	
Nominal value (μ_T)	Observed range ($\approx \pm 3\sigma_T$)	Nominal value (μ_P)	Observed range ($\approx \pm 3\sigma_P$)	Nominal value (μ_D)	Observed range ($\approx \pm 3\sigma_D$)
630	±7	4	±10	11	±0.02
700	±7	100	±10	13	±0.02
750	±6	200	±20	15	±0.02
800	±6	300	±20	17	±0.02
850	±6	400	±20	19	±0.02
		500	±40	21	±0.02
		600	±40		

Table 4: Optimal process conditions for maximizing expected yield of nanostructures

Nanostructure	Temperature	Pressure	Distance
Nanosaws	630	307	15.1
Nanowires	695	113	19.0
Nanobelts	683	4	17.0

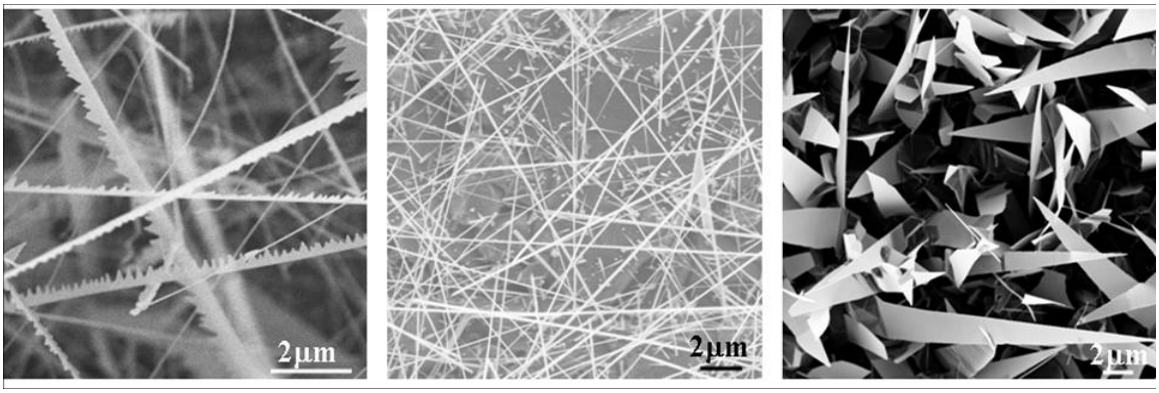

Figure 1 : SEM images of nanostructures

(From the left : Nanosaws, nanowires and nanobelts)

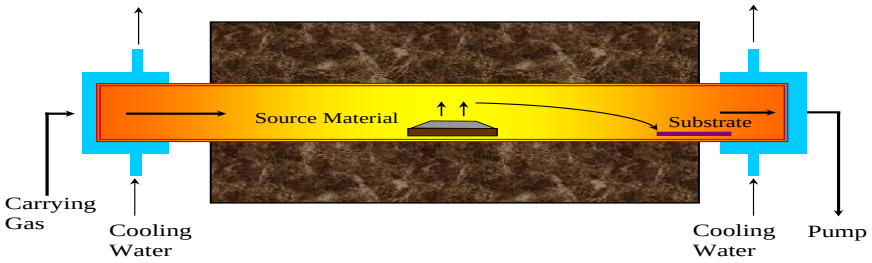

Figure 2 : The synthesis process

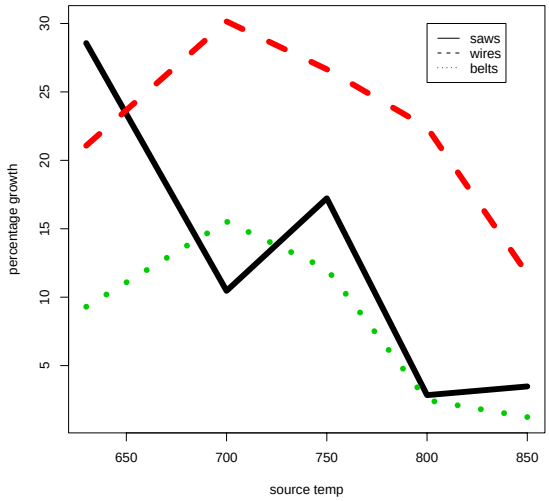

Figure 3a : Growth vs Temperature

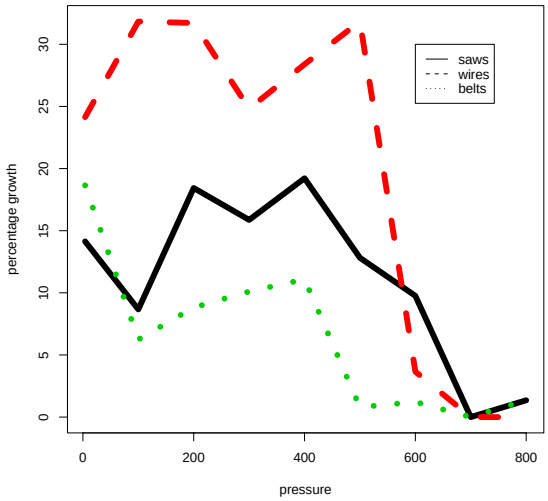

Figure 3b : Growth vs Pressure

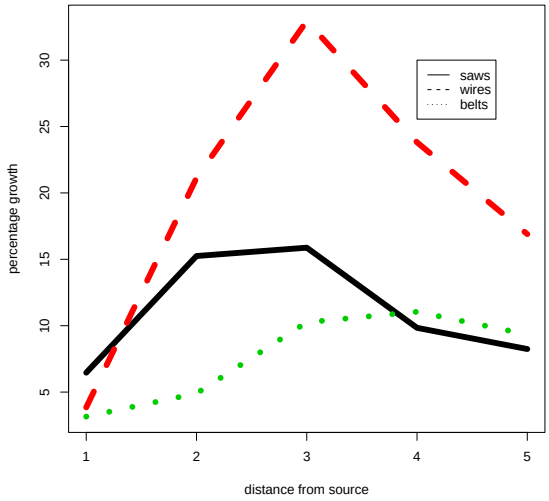

Figure 3c : Growth vs Distance

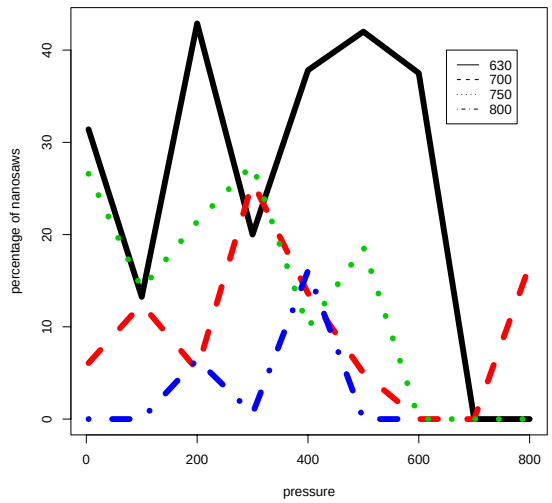

Figure 4a : $TEMP \times PRES$ for nanosaw growth

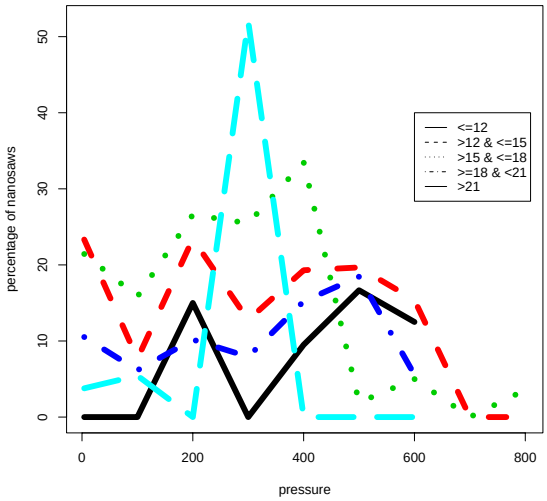

Figure 4b : $PRES \times DIST$ for nanosaw growth

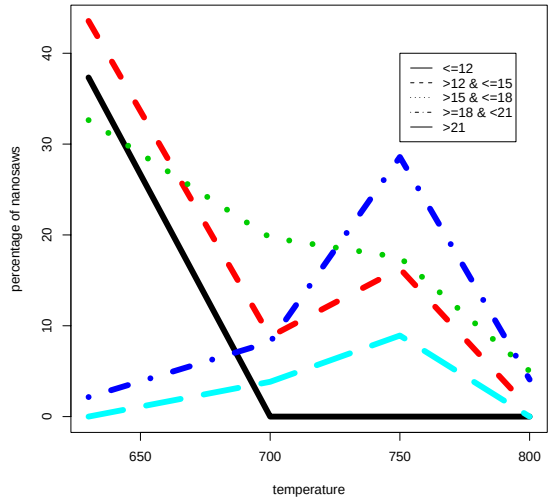

Figure 4c : $DIST \times TEMP$ for nanosaw growth

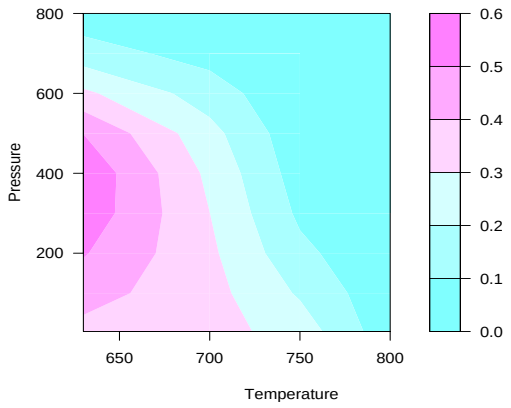

Figure 5a : Average probability of nanosaws at 15 cm

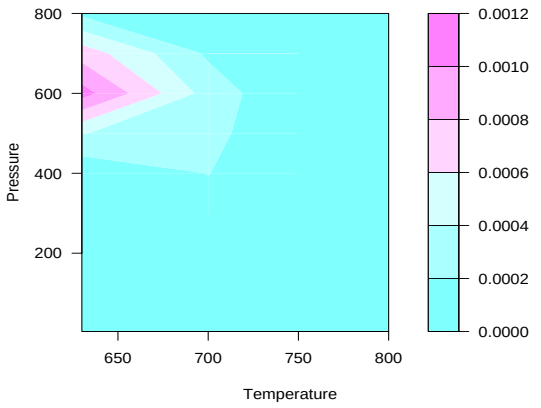

Figure 5b : Variance of probability of nanosaws at 15 cm

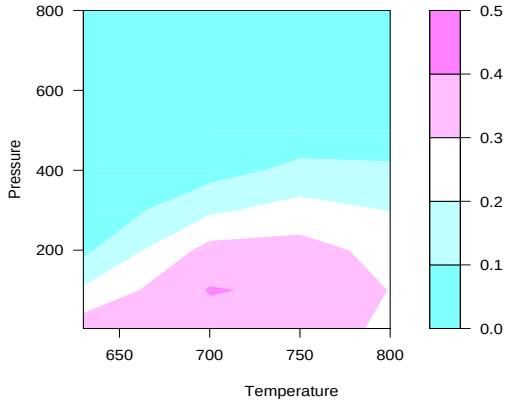

Figure 5c : Average probability of nanowires at 19 cm

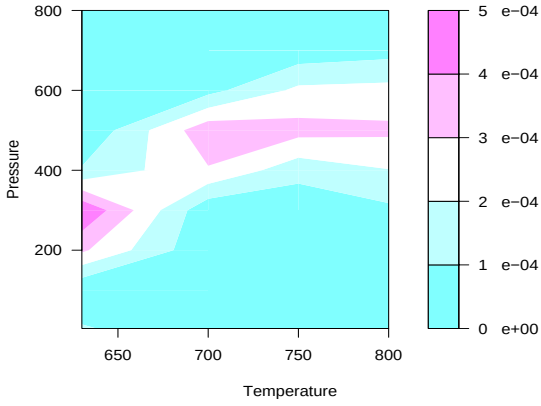

Figure 5d : Variance of probability of nanowires at 19 cm

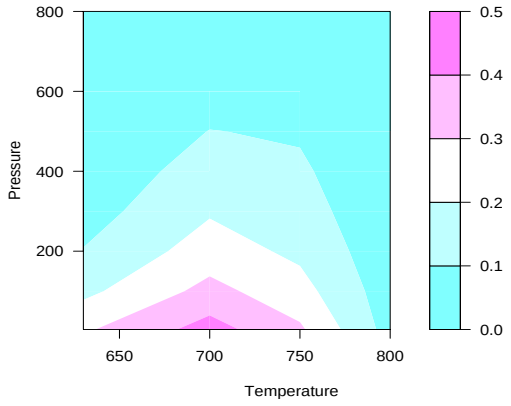

Figure 5e : Average probability of nanobelts at 17 cm

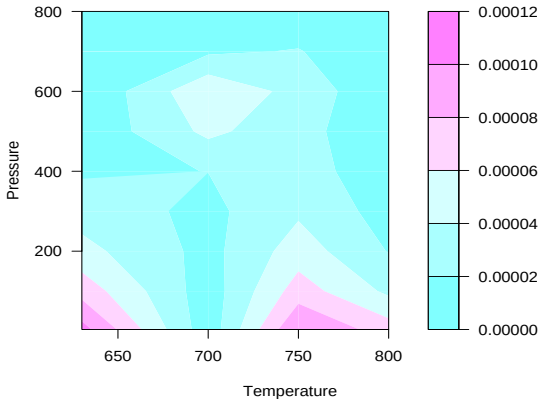

Figure 5f : Variance of probability of nanobelts at 17 cm